Computer-Aided Drug Design

Deutsche Ausgabe: DOI: 10.1002/ange.201507320
Internationale Ausgabe: DOI: 10.1002/anie.201507320

Optimization of TRPV6 Calcium Channel Inhibitors Using a 3D Ligand-Based Virtual Screening Method

Céline Simonin, Mahendra Awale, Michael Brand, Ruud van Deursen, Julian Schwartz, Michael Fine, Gergely Kovacs, Pascal Häfliger, Gergely Gyimesi, Abilashan Sithampari, Roch-Philippe Charles, Matthias A. Hediger, and Jean-Louis Reymond**

Abstract: *Herein, we report the discovery of the first potent and selective inhibitor of TRPV6, a calcium channel overexpressed in breast and prostate cancer, and its use to test the effect of blocking TRPV6-mediated Ca^{2+}-influx on cell growth. The inhibitor was discovered through a computational method, xLOS, a 3D-shape and pharmacophore similarity algorithm, a type of ligand-based virtual screening (LBVS) method described briefly here. Starting with a single weakly active seed molecule, two successive rounds of LBVS followed by optimization by chemical synthesis led to a selective molecule with 0.3 μM inhibition of TRPV6. The ability of xLOS to identify different scaffolds early in LBVS was essential to success. The xLOS method may be generally useful to develop tool compounds for poorly characterized targets.*

Virtual screening can valuably assist drug discovery whenever a large body of information is already available, such as the activity and selectivity profiles of hundreds of potent inhibitors of the desired target or its high-resolution crystal structure.[1] On the other hand, small molecule inhibitors are often needed to understand the biological role of poorly characterized targets, in particular to selectively shut down their activity on a short time-scale and test if the effects observed by genetic knock-out are indeed caused by loss of function.[2] Herein, we report the application of virtual screening to such a problem at the example of transient receptor potential vanilloid 6 (TRPV6), a selective calcium channel overexpressed in advanced prostate cancer tissues and carcinomas of the colon, breast, thyroid, and ovary.[3] A decreased proliferation rate was observed for prostate and breast cancer cells upon siRNA knockdown of TRPV6, suggesting that cancer cell proliferation might be controllable by inhibition of calcium transport through this channel.[4] Although several small molecule inhibitors of TRPV6 have indeed been shown to reduce cell growth, these compounds only inhibited calcium transport at high micromolar concentration, and were non-selective versus the close analogues TRPV5 and store-operated calcium channels, precluding a conclusive link between TRPV6 calcium transport function and cell growth.[5]

TRPV6 is assumed to adopt the six transmembrane domain structure typical of TRP family channels.[3g] A homology model derived from the recently reported rat TRPV1 crystal structure suggests that a hydrophobic binding pocket analogous to the binding site postulated for capsaicin in TRPV1[6] and suitable for small molecule binding might exist in TRPV6 (Supporting Information, Figure S1). The absence of an experimental structure, however, precluded the use of structure-based methods for ligand design.[1b,7] We therefore set out to test if ligand-based virtual screening (LBVS)[1c] might be used to discover a potent and selective small molecule TRPV6 inhibitor starting from the available weak TRPV6 inhibitors **1–5** as seed compounds (Figure 1D, the covalent non-selective channel inhibitor 2-aminoethyl phenylboronate was not considered).[5] Since it was not known which part of these inhibitors contributed to their TRPV6 activity, we searched for an LBVS method capable of identifying similarities to part or the whole of a seed molecule, if possible favoring rather small, ligand-efficient fragments for screening,[8] and emphasizing scaffold hopping[9] since the scaffolds of the weakly active seed molecules were probably not optimal.

The ligand overlap score (LOS), which quantifies the spatial overlap between two molecules as the weighted sum of atom pair proximity scores, was selected as a substructure-independent metric of shape similarity between two molecules.[10] LOS was computed separately for hydrophobic atoms, hydrogen bond donor and acceptor atoms which were previously found to be useful atom categories for pharmacophore fingerprint design.[11] Only the lowest energy conformer generated by CORINA[12] was used as 3D-model of each molecule because sampling multiple conformers would increase computational costs by at least 100-fold and has been shown to not yield clear performance benefits in related 3D LBVS methods.[13] The combined score was maximized by alignment and iterative translation and rotation of query relative to seed molecule along their principal molecular axes (Figure 1A–C; Supporting Information, Figure S2). The resulting algorithm xLOS (atom category *e*xtended *L*igand *O*verlap *S*core) performed comparably well to other 3D LBVS methods for the recovery of actives from inactive decoy molecules in various sets of bioactive

[*] Dr. C. Simonin, Dr. M. Awale, M. Brand, Dr. R. van Deursen, Dr. J. Schwartz, Prof. Dr. J.-L. Reymond
Department of Chemistry and Biochemistry
National Center of Competence in Research NCCR TransCure
University of Bern, Freiestrasse 3, 3012 Bern (Switzerland)
E-mail: jean-louis.reymond@dcb.unibe.ch
Dr. M. Fine, Dr. G. Kovacs, P. Häfliger, Dr. G. Gyimesi, A. Sithampari, Prof. Dr. R.-P. Charles, Prof. Dr. M. A. Hediger
Institute of Biochemistry and Molecular Medicine
National Center of Competence in Research NCCR TransCure
University of Bern, Bühlstrasse 28, 3012 Bern (Switzerland)
E-mail: matthias.hediger@ibmm.unibe.ch

Supporting information for this article is available on the WWW under http://dx.doi.org/10.1002/anie.201507320.

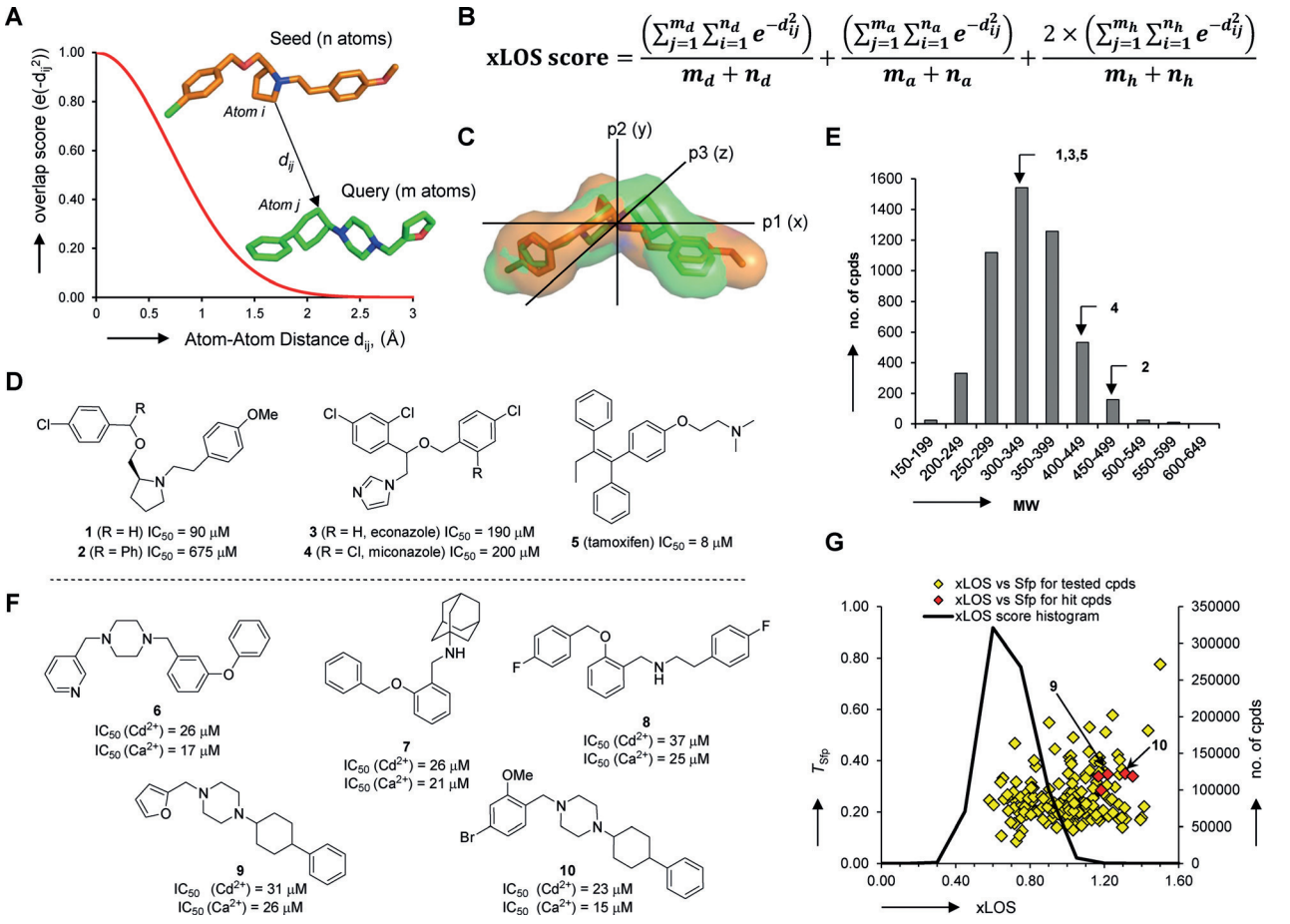

Figure 1. LBVS with xLOS and its application to TRPV6. A) Atom pair proximity score. B) xLOS combines LOS for H-bond donor (d), H-bond acceptor (a), and hydrophobic atoms (h). C) Alignment of seed (**1**, orange) and query (**9**, green) molecule after xLOS value optimization by iterative translations and rotation along the principal molecular axes p1-p2-p3. D) Structures of known TRPV6 inhibitors. E) MW histogram of top xLOS scoring compounds. F) Structure of hits **6–10** identified after the first round of LBVS. IC_{50} values were determined with pure compounds (see the Supporting Information). G) Scatter plot of substructure similarity versus xLOS score for tested compounds (yellow) and active hits (red, hit rate: 4%), and xLOS histogram of the 800 000 cpds analyzed by LBVS.

molecules from the directory of useful decoys (Supporting Information, Figure S3).[11,13b,14] Furthermore, xLOS showed significant scaffold-hopping, indicated by the fact that bioactive analogues were retrieved by xLOS independent of their substructure similarity to the seed compound used for LBVS (Supporting Information, Figure S4).[9] This effect may be attributed to the fact that xLOS perceives shape and pharmacophores by atom positions only without considering connectivity patterns.

xLOS was used to score ~800 000 purchasable small molecules against seed inhibitors **1–5** (Figure 1 D).[15] Because xLOS penalizes non-overlapping parts of seed and query molecule by scaling to molecular size (Figure 1 B), high-scoring molecules generally had a relatively small size favorable for hit compounds (Figure 1 E).[16] The five lists of 1000 top scoring hits were clustered to select diverse molecules avoiding pan assay interference compounds,[17] and 133 compounds were purchased for experimental evaluation. Testing inhibition of TRPV6-induced Ca^{2+} and Cd^{2+} influx in transiently transfected HEK293 cells (Supporting Information, Figures S5, S6)[18] revealed five weakly active hits (**6–10**, IC_{50} ~ 20 μM), with very different scaffolds compared to the seed molecules (Figure 1 F/G).

Hits **6–10** were used as seeds for a second LBVS round using both xLOS and a conventional substructure fingerprint similarity search,[19] and an additional 90 analogues were purchased and tested. While all analogues of hits **6–8** were inactive, precluding optimization, 16 analogues of hits **9** and **10** (**11 a-p**) were active, indicating that their common (4-phenylcyclohexyl)piperazine scaffold was suitable for further exploration. Both of these compounds originated from a scaffold-hopping step from prolinol type seed **1** in the first LBVS round. Separation of the *cis*/*trans* diastereomers in the second round of LBVS hits **11 a–g** revealed a consistently stronger activity in *cis*-diastereomers, with the best activity reached with compound *cis*-**11 a** identified by xLOS (Figure 2 A/B; Supporting Information, Figure S7).

Inhibitor *cis*-**11 a** was further optimized by synthesizing analogues by reductive alkylation of various 4-aryl-cyclohexanones with different mono-substituted piperazines and analogues (Scheme 1). Variations in ring A led to stronger inhibition by removing the methylene group between ring A

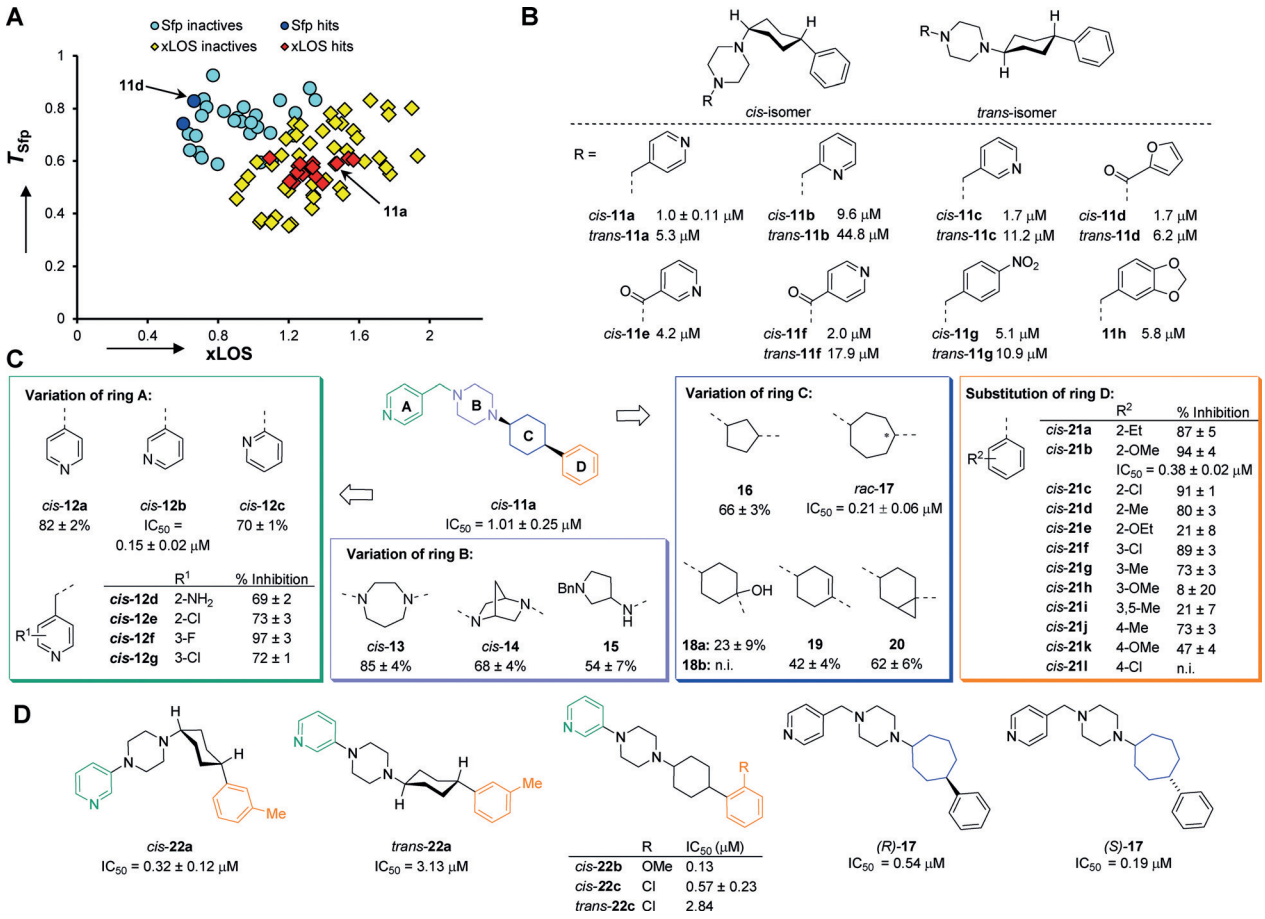

Figure 2. Optimization of TRPV6 inhibitors. A) Scatter plot of substructure similarity (T_{Sfp}) versus xLOS score in 2nd round LBVS (highest value relative to seeds **6**–**10**). Hits defined as ≥70% inhibition of Cd^{2+} influx in *h*TRPV6 transfected HEK293 cells. Hit rate xLOS: 20%, Sfp: 8%. B) Structure and IC_{50} values for Cd^{2+} influx of hits highlighted in (A). C) Synthetic analogues of *cis*-**11a**. Activity on *h*TRPV6 given as % inhibition of Cd^{2+} influx at 5 μM (3 replicates) or IC_{50} value (7 concentrations × 6 replicates), as mean ± SEM for $n \geq 2$. D) Structures and activities of optimized inhibitors TRPV6 **22a-c** and diastereomeric mixtures (*R*)- and (*S*)-**17**.

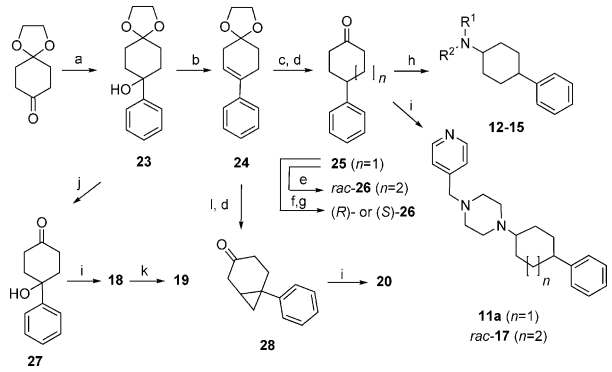

Scheme 1. Synthesis of **11a** and analogues.Conditions: a) PhMgBr, THF, reflux, 30 min (quant.). b) TsOH, toluene, reflux, 4 h. c) H_2, Pd/C, EtOAc, RT, 18 h. d) HCl, acetone, reflux, 18 h (**25**, 44% over 3 steps; **28**, 42% over 3 steps). e) Me_3SiCHN_2, *n*BuLi, MeOH, SiO_2, Et_2O, THF, −78 °C→RT, 1 h30 (48%). f) N_2CHCO_2Et, (*R*)- or (*S*)-3,3′-bis(trimethylsilyl)-1,1′-binaphtyl-2,2′-diol, Me_3Al, toluene, −78 °C, 24 h. g) LiCl, DMSO, 160 °C, 3 h (32-39% over 2 steps). h) Secondary amine, $NaBH(OAc)_3$, DCE, RT, 20 h (4-49%). i) 1-((pyridin-4-yl)methyl)piperazine, $NaBH(OAc)_3$, DCE, RT, 20 h (*cis*-**11a**, 17%; *trans*-**11a**, 5%; *rac*-**17**, 22%; **18**, 40%; **20**, 26%). j) HCl, THF, RT, 21 h (65%). k) HCl, H_2O, reflux, 15 h (72%). l) $ZnEt_2$, TFA, CH_2I_2, DCM, 2 h (47%).

and the piperazine core (**12a**), and moving the nitrogen to the meta position (**12b**), while further substitutions of the pyridine ring (**12d–g**) did not affect the activity (Figure 2C). Note that the *ortho*-pyridine analogue **12c** reported as sterol isomerase inhibitor (*cis*: $K_i = 50$ nM, *trans*: $K_i = 17$ nM),[20] was also weakly active as a TRPV6 inhibitor (*cis*: 72% at 5 μM). Activity was reduced by modifying piperazine ring B (**13**–**15**). Variations in cyclohexane ring C were also detrimental (**16**, **18**–**20**), however ring expansion to a seven-membered ring gave the more potent chiral analogue **17** as a mixture of four stereoisomers. A synthesis starting from cycloheptanones (*R*)-**26** (99% *ee*) and (*S*)-**26** (96% *ee*)[21] yielded two inseparable pairs of diastereomers (*R*)- and (*S*)-**17** with comparable activities. Substitution of ring D was also explored leading to improvements with the 2-methoxy (*cis*-**21b**) analogues. Variations in rings A and D were combined to obtain *cis*-**22a-c** as optimized, potent TRPV6 inhibitors (Figure 2D; Supporting Information, Figure S8).

Inhibitor *cis*-**22a** was investigated in detail and showed high selectivity against other calcium channels and related TRP targets (Table 1; Supporting Information, Figure S1). Although similarity searches in ChEMBL followed by

Table 1: In vitro pharmacology profile of *cis*-**22a** on several ion channels.[a]

Channel	% Inh. at 10 μM
TRPV1 (agonist effect) (*h*)	−15.5 ± 0.7[b]
TRPV1 (antagonist effect) (*h*)	29.6 ± 8.6
TRPV3 (antagonist effect) (*h*)	−11.5 ± 2.0
TRPV5 (antagonist effect) (*r*)	79.9 ± 1.4 (IC_{50} = 2.4 μM)
TRPM8 (agonist effect) (*h*)	−7.4 ± 1.4[b]
TRPM8 (antagonist effect) (*h*)	21.2 ± 7.5
Store-operated Ca^{2+} channels	−10.1 ± 6.0

[a] The agonist or antagonist effect of *cis*-**22a** on TRP channels was measured in a functional assay by recording calcium mobilization. [b] % of control agonist response. *h*, human; *r*, rat. See also Supporting Information, Table S1.

experimental validation identified significant cross-inhibition of dopamine, muscarinic, opiate μ, and serotonin GPCRs typical for aromatic piperazines and of the cardiac potassium channel hERG (23–98% at 10 μM; Supporting Information, Table S1), *cis*-**22a** was judged suitable for testing the effect of TRPV6 inhibition on cell growth. The anti-proliferative activity of *cis*-**22a** was investigated on TRPV6 expressing T47D human breast cancer cells and TRPV6 non-expressing SKOV3 ovarian carcinoma cells (Figure 3A). Treatment of

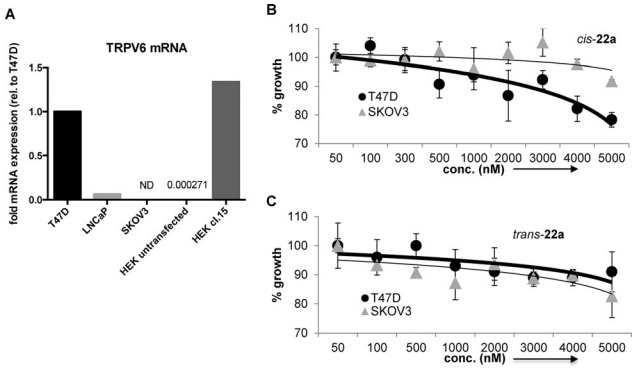

Figure 3. Antiproliferative activity of *cis*-**22a** and *trans*-**22a** on TRPV6 positive (T47D) and TRPV6 negative (SKOV3) breast cancer cells. A) Expression of TRPV6 in different cell lines. B, C) Percent of control cell growth at day 6 as a function of increasing inhibitor concentration.

T47D cells with *cis*-**22a** decreased cellular proliferation by 20% at 5 μM (IC_{50} = 25 ± 10 μM), a concentration sufficient to block TRPV6-mediated Ca^{2+} influx, while SKOV3 cells were unaffected (IC_{50} > 50 μM, Figure 3B). By contrast, there was no significant growth difference between the two cells lines when treated with the less potent diastereomer *trans*-**22a** (Figure 3C). The selective but significantly smaller effect of *cis*-**22a** compared to siRNA knockdown (50% reduction in cell growth)[4b] suggests that TRPV6 affects cell growth by other mechanisms than the Ca^{2+} uptake from the extracellular medium inhibited by *cis*-**22a**, in line with a recent report of its role in store operated calcium entry.[4c]

In summary the potent and selective TRPV6 inhibitor *cis*-**22a** with a (4-phenylcyclohexyl)piperazine scaffold was obtained starting from the weakly active prolinol-based inhibitor **1** by two successive rounds of LBVS, followed by optimization by synthesis. While achieving useful hit rates (round 1: 4%, round 2: 20%), xLOS selected high scaffold diversity and allowed transition from the weakly active seed **1** to a more favorable scaffold early in the optimization campaign. In contrast to many virtual screening approaches requiring large amounts of information to get started, xLOS can start from a single seed and does not require detailed structural information on its target or any pre-existing structure–activity relationship data. It should also be noted that scanning purchasable collections was not sufficient, and that chemical synthesis was critical to obtain a potent inhibitor in the later stages of optimization. The method should be generally useful to support the investigation of targets for which only weak or unselective inhibitors have been documented.

Acknowledgements

This work was supported financially by the Swiss National Science Foundation, NCCR TransCure. MF and GG were supported by the Marie Curie Actions International Fellowship Program (IFP) TransCure.

Keywords: calcium channels · drug discovery · TRP channels · virtual screening

How to cite: *Angew. Chem. Int. Ed.* **2015**, *54*, 14748–14752
Angew. Chem. **2015**, *127*, 14961–14965

[1] a) G. Klebe, *Drug Discovery Today* **2006**, *11*, 580–594; b) T. Scior, A. Bender, G. Tresadern, J. L. Medina-Franco, K. Martinez-Mayorga, T. Langer, K. Cuanalo-Contreras, D. K. Agrafiotis, *J. Chem. Inf. Model.* **2012**, *52*, 867–881; c) K. Heikamp, J. Bajorath, *Chem. Biol. Drug Des.* **2013**, *81*, 33–40; d) M. Reutlinger, T. Rodrigues, P. Schneider, G. Schneider, *Angew. Chem. Int. Ed.* **2014**, *53*, 582–585; *Angew. Chem.* **2014**, *126*, 593–596.

[2] J. Blagg, P. Workman, *Curr. Opin. Pharmacol.* **2014**, *17*, 87–100.

[3] a) J. B. Peng, X. Z. Chen, U. V. Berger, P. M. Vassilev, H. Tsukaguchi, E. M. Brown, M. A. Hediger, *J. Biol. Chem.* **1999**, *274*, 22739–22746; b) L. Yue, J. B. Peng, M. A. Hediger, D. E. Clapham, *Nature* **2001**, *410*, 705–709; c) M. A. Hediger, E. M. Brown, J. B. Peng, *Patent*, US6534642, **2003** and US7078178, **2006**; d) D. E. Clapham, L. W. Runnels, C. Strubing, *Nat. Rev. Neurosci.* **2001**, *2*, 387–396; e) K. A. Bolanz, G. G. Kovacs, C. P. Landowski, M. A. Hediger, *Mol. Cancer Res.* **2009**, *7*, 2000–2010; f) C. Fecher-Trost, P. Weissgerber, U. Wissenbach, *Handb. Exp. Pharmacol.* **2014**, *222*, 359–384; g) U. A. Hellmich, R. Gaudet, *Handb. Exp. Pharmacol.* **2014**, *223*, 963–990.

[4] a) V. Lehen′kyi, M. Flourakis, R. Skryma, N. Prevarskaya, *Oncogene* **2007**, *26*, 7380–7385; b) K. A. Bolanz, M. A. Hediger, C. P. Landowski, *Mol. Cancer Ther.* **2008**, *7*, 271–279; c) M. Raphaël, V. y. Lehen′kyi, M. Vandenberghe, B. Beck, S. Khalimonchyk, F. Vanden Abeele, L. Farsetti, E. Germain, A. Bokhobza, A. Mihalache, P. Gosset, C. Romanin, P. Clézardin, R. Skryma, N. Prevarskaya, *Proc. Natl. Acad. Sci. USA* **2014**, *111*, E3870–E3879.

[5] a) C. Landowski, K. Bolanz, A. Y. Suzuki, M. A. Hediger, *Pharm. Res.* **2011**, *28*, 322–330; b) G. Kovacs, N. Montalbetti, A. Simonin, T. Danko, B. Balazs, A. Zsembery, M. A. Hediger, *Cell Calcium* **2012**, *52*, 468–480; c) A. Hofer, G. Kovacs, A.

Zappatini, M. Leuenberger, M. A. Hediger, M. Lochner, *Bioorg. Med. Chem.* **2013**, *21*, 3202 – 3213.
[6] E. Cao, M. Liao, Y. Cheng, D. Julius, *Nature* **2013**, *504*, 113 – 118.
[7] M. Lill, *Methods Mol. Biol.* **2013**, *993*, 1 – 12.
[8] A. L. Hopkins, G. M. Keseru, P. D. Leeson, D. C. Rees, C. H. Reynolds, *Nat. Rev. Drug Discovery* **2014**, *13*, 105 – 121.
[9] G. Schneider, W. Neidhart, T. Giller, G. Schmid, *Angew. Chem. Int. Ed.* **1999**, *38*, 2894 – 2896; *Angew. Chem.* **1999**, *111*, 3068 – 3070.
[10] a) S. K. Kearsley, G. Smith, *Tet. Comput. Methodol.* **1990**, *3*, 615 – 633; b) E. A. Kennewell, P. Willett, P. Ducrot, C. Luttmann, *J. Comput.-Aided Mol. Des.* **2006**, *20*, 385 – 394; c) P. C. Hawkins, A. G. Skillman, A. Nicholls, *J. Med. Chem.* **2007**, *50*, 74 – 82.
[11] M. Awale, X. Jin, J. L. Reymond, *J. Cheminf. J. Cheminform.* **2015**, *7*, 3.
[12] J. Sadowski, J. Gasteiger, *Chem. Rev.* **1993**, *93*, 2567 – 2581.
[13] a) S. Renner, C. H. Schwab, J. Gasteiger, G. Schneider, *J. Chem. Inf. Model.* **2006**, *46*, 2324 – 2332; b) V. Venkatraman, V. I. Perez-Nueno, L. Mavridis, D. W. Ritchie, *J. Chem. Inf. Model.* **2010**, *50*, 2079 – 2093.
[14] N. Huang, B. K. Shoichet, J. J. Irwin, *J. Med. Chem.* **2006**, *49*, 6789 – 6801.
[15] J. J. Irwin, T. Sterling, M. M. Mysinger, E. S. Bolstad, R. G. Coleman, *J. Chem. Inf. Model.* **2012**, *52*, 1757 – 1768.
[16] a) M. M. Hann, *MedChemComm* **2011**, *2*, 349 – 355; b) N. Foloppe, *Future Med. Chem.* **2011**, *3*, 1111 – 1115.
[17] J. B. Baell, G. A. Holloway, *J. Med. Chem.* **2010**, *53*, 2719 – 2740.
[18] G. Kovacs, T. Danko, M. J. Bergeron, B. Balazs, Y. Suzuki, A. Zsembery, M. A. Hediger, *Cell Calcium* **2011**, *49*, 43 – 55.
[19] a) P. Willett, *Drug Discovery Today* **2006**, *11*, 1046 – 1053; b) M. Awale, J. L. Reymond, *Nucleic Acids Res.* **2014**, *42*, W234 – W239.
[20] F. Berardi, C. Abate, S. Ferorelli, A. F. de Robertis, M. Leopoldo, N. A. Colabufo, M. Niso, R. Perrone, *J. Med. Chem.* **2008**, *51*, 7523 – 7531.
[21] T. Hashimoto, Y. Naganawa, K. Maruoka, *J. Am. Chem. Soc.* **2011**, *133*, 8834 – 8837.

Received: August 6, 2015
Revised: September 2, 2015
Published online: October 12, 2015

